2. ACCELERATOR AUGMENTATION PROGRAM

2.1 HIGH CURRENT INJECTOR

The High Current Injector (HCI) Project will accelerate the ion beam from ECR source using normal temperature Radio-Frequency Quadrupole (RFQ), IH type Drift Tube Linac (DTL) and superconducting low beta cavity module to match the input velocity at our existing superconducting linear accelerator.

2.1.1 High Temperature Superconducting ECRIS -PKDELIS and Low Energy Beam Transport (LEBT)

G. Rodrigues, Sarvesh Kumar, Y. Mathur, P. Barua, A. Kothari, M. Archunan, Chandra Pal, R. Ahuja, A.J. Malyadri, U. K. Rao, R.N. Dutt, A. Mandal & D. Kanjilal

a) Testing of the 18 GHz High Temperature Superconducting ECR ion source, PKDELIS and Low Energy Beam Transport System on the 200 kV high voltage platform

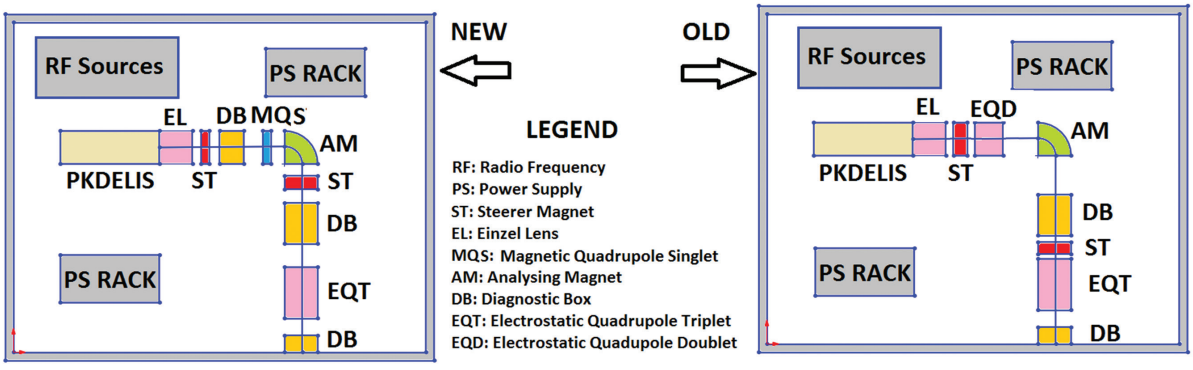

Fig. 2.1.1 View of the low energy beam transport schematics on the 200 kV high voltage platform for the first (old) and second (new) configurations.

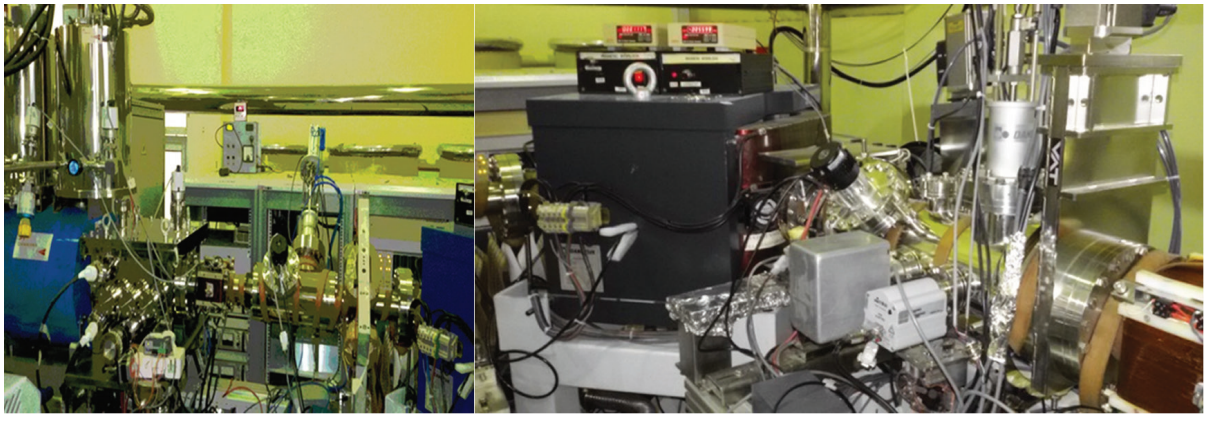

Fig. 2.1.2 (left)View of the modified beamline (second configuration) between ion source and analysing magnet (right) view of part of post-analyzing section

In the first configuration of the installed LEBT shown in Figure 2.1.1, it was observed that the beam could not be steered in the dispersive plane at the location of the diagnostic box placed after the analyzing magnet. The beam was offset from the x fiducial by more than 26 mm. Due to the absence of any diagnostic elements before the analysing magnet, it was difficult to visualize the beam during beam tuning. The electrostatic quadrupole doublet was found effective with only one of the quadrupoles, while the other quadrupole was normally found to be set to 0 V. Therefore, in order to circumvent these problems, an improved alternate configuration was implemented.

In the second configuration, the electrostatic quadrupole doublet was replaced with a magnetic quadrupole singlet which was placed closer to the analyzing magnet to get most of the beam through. A compact diagnostic box consisting of a Faraday cup and beam profile monitor was positioned just after the multi-electrode extraction system. An additional steerer (x-steerer) was placed on the bellow after the analyzing magnet for steering the beam in the dispersive plane. During the first tests with the new configuration, it was observed that the beam could be steered at the diagnostic location, but the beam was defocusing while being steered. This was attributed to the field in-homogeneity of the x-steerer. This is presently being modified to further improve it.

The beam transmission at the position of the diagnostic box after the analyzing magnet was measured to be ~ 80 %, nearly 100 % at the third Faraday cup, while the beam transmission at the first Faraday cup was only a small fraction of the drain current with the drain current being a factor of 10 lower. This will be further improved by improving the vacuum on the injection side of the ion source and further reducing the distance between the ion source and the analyzing magnet.

b) Electronics and related maintenance activities

Python-based online scanning of charge state distributions

An online automatic logging and scanning of charge state distributions, has been developed for the 18 GHz HTS ECR ion source, PKDELIS. A python QT based GUI client program fetches the value of magnetic field in Gauss from the Tesla-meter which is interfaced through RS232 to VME control system server (placed on the high voltage platform) by varying the current in the analyzer magnet and observing the Faraday cup current value (Figure 2.1.3 & 2.1.4). It then plots the magnetic field v/s FC current with the user specified resolution (number of steps). Some of the features involve:

1. User-friendly GUI software written in python
2. Easy calibration, saving of data as per user's choice
3. Parameter v/s time plot
4. Sweep Analysis (Field v/s current plot)
5. Beam selection based on live *m/q* data
6. Multiple time synchronized plots

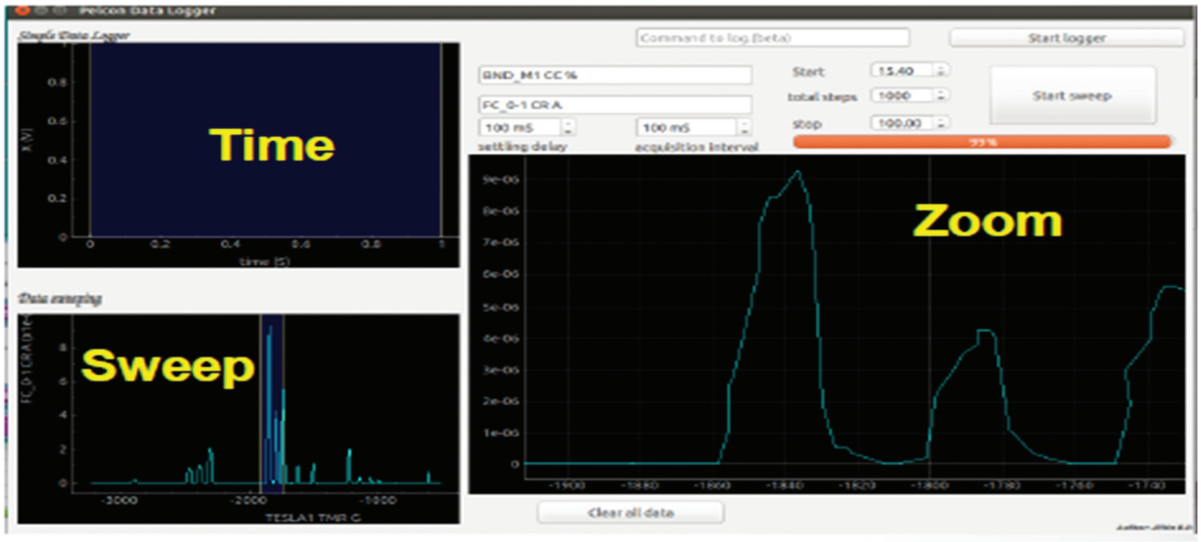

Fig. 2.1.3 View of the python based, online charge state distribution

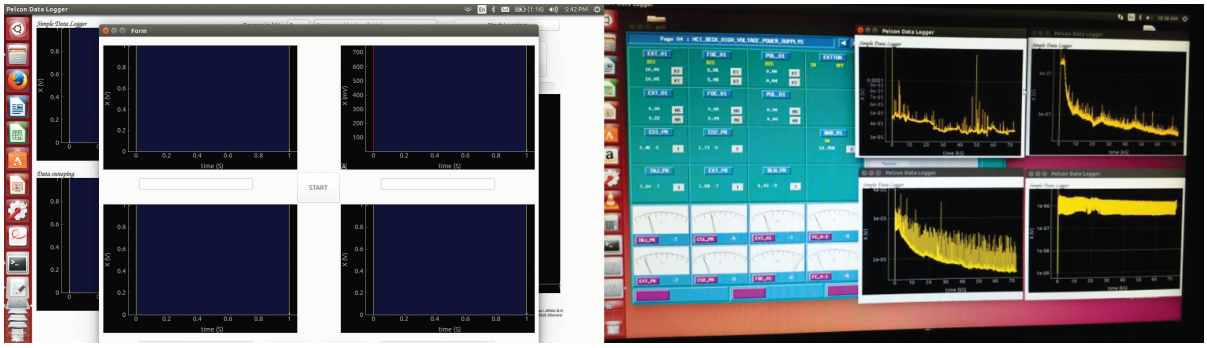

Fig. 2.1.4 View of the python based, multiple time synchronized plots

Instrument interfacing with pserv for operating a wide band traveling wave tube (TWT) amplifier

The 18 GHz klystron is presently used for powering the 18 GHz high temperature superconducting ECR ion source. Alternatively, a wide band travelling wave tube (TWT) amplifier is being bought as a back-up in the eventuality of a breakdown of the klystron, so that the injector is kept running for experiments. Therefore, instruments like RF power amplifier and signal generator (RF Oscillator) placed on the high voltage platform have been interfaced to VME based control system server *pserv* so that they are controllable through *pcli*. NI GPIB-RS232 converter has been used to connect both devices in parallel to the same server (Figure 2.1.5). Frequency, RF Level and ON/OFF control for signal generator while forward, reflected power, TWT temperature readback with Standby, Operate, System ON/OFF commands can be fired for RF Power amplifier using the GPIB through *pserv/pcli.*

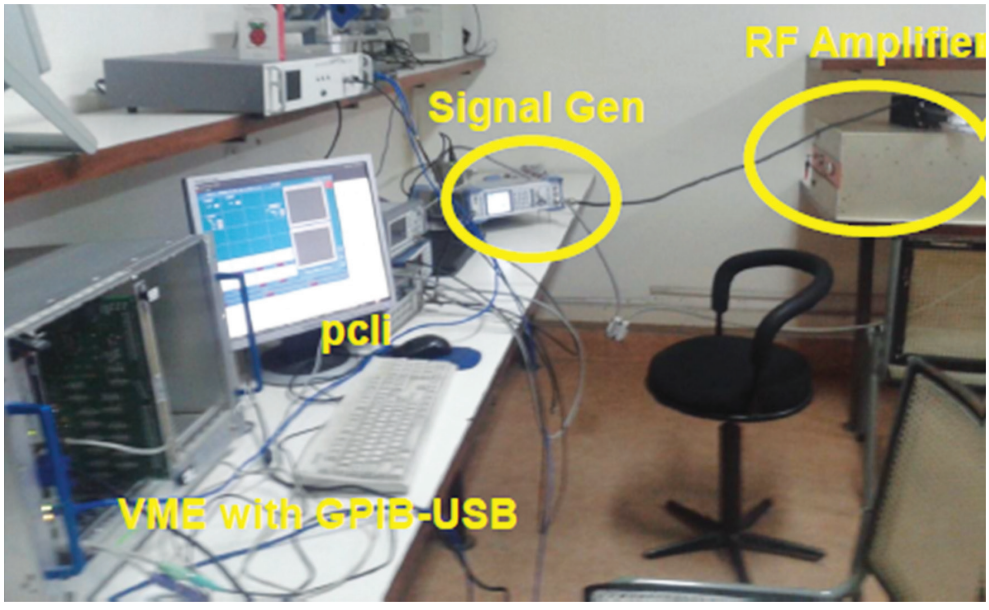

Fig. 2.1.5 Interfacing with *pserv* for operating a TWT amplifier

2.1.2 Assembly and low power RF tests on the modulated 2.5m RFQ Accelerator

Sugam Kumar, R. Ahuja, A. Kothari, C.P. Safvan

A high current injector (HCI) is being developed at Inter University Accelerator Centre to inject highly charged ions into the superconducting LINAC. The ion beams of $A/q \leq 6$ produced by the ECR ion source will be injected into a 48.5 MHz, 4-rod Radio Frequency Quadrupole (RFQ). The RFQ is designed to accelerate ions from 8 keV/amu to 180 keV/amu energy.

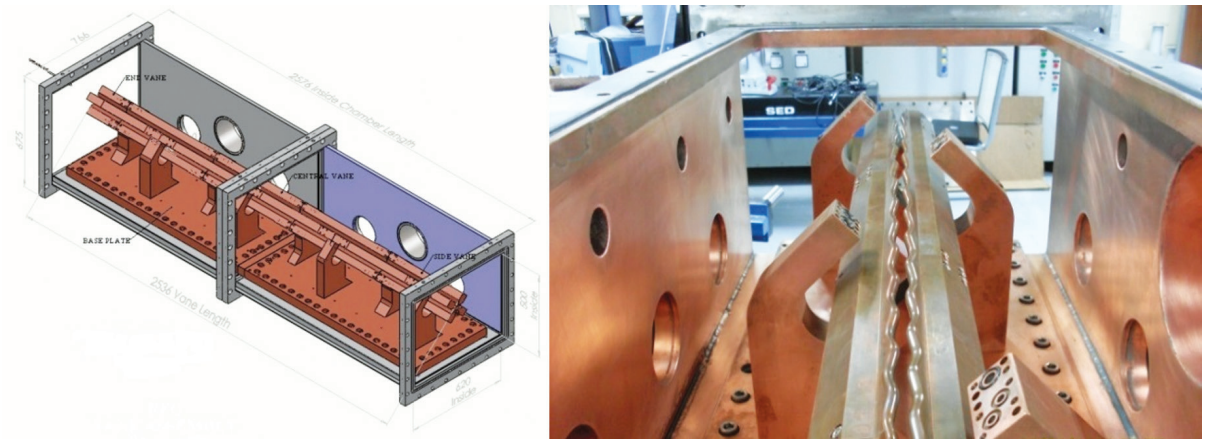

Fig 2.1.6 A three dimensional inside view of Radio Frequency Quadrupole

A view of the RFQ is shown in Fig.2.1.6 during assembly of the modulated vanes. The electrodes are in the form of four-rod structure. The length of the electrodes is 2.536 meters with bore diameter of 12 mm. The whole electrode assembly is inserted into the RFQ cavity. The electrodes, electrode supporting posts and base plate are made of copper while chamber is made of stainless steel material. To improve the quality factor the inner surface of the chamber is copper plated with a plating thickness of 70 microns. The cavity is equipped with various ports where the input inductive loop for power coupling and output loop for probe are installed. The input loop is movable and its position can be adjusted to achieve proper impedance matching between the RFQ system and the RF power source. The system is able to achieve high vacuum level (10^{-7} Torr) with the help of a turbo molecular pump. The results of the RF measurements are given in the following section. The beam optics and cavity design were done using LIDOS and CST Microwave Studio. The 3D CAD drawing of the RFQ electrodes assembly and its cavity for mechanical construction are done using SolidWorks.

Following the mechanical alignment, the vanes were installed and were made ready for the low level RF tests. The perturbed resonance frequency (f), quality factor (Q) and unperturbed resonance frequency (f_0) were measured with the network analyzer. The measured value of Q using 3 dB method was 5524. This quality factor was achieved without any special surface treatment and without RF seals. This value of Q was used throughout in the later calculations. Self-exciting loop is used to minimize the possible long-term temperature drift while measuring the frequency shift.

Table 1: RF parameters of final 4-rod RFQ

RF Parameters	Designed Value	Simulated	Experimental
Resonance Frequency (f0)	48.5 MHz	-	44.12
Quality Factor (Q)	-	-	5524
Shunt impedance (Rsh)	-	90k-ohm	87 k-ohm
Power Required (Pin)	-	-	80 kW/m

The frequency shift along the length of the cavity is shown in Fig.2.1.7. For most of the measurements, the bead was a 2 mm diameter sapphire and fishing thread of 0.28 mm diameter was used. The bead was spherical in shape, and is extremely sensitive to the electric field. Two independent measurements were made in the azimuthal plane to check the quadrupole symmetry and the electric field distribution. The result of the bead pull along the azimuthal plane is shown in Figure 2.1.7. The graph indicates that the distribution of the electric field is symmetrical within the beam radius and tends to become asymmetrical in region greater than the beam radius.

It was found that the electric field is flat within ±2% in the transverse plane while in longitudinal direction the electric field is flat within ±6%. This non uniform distribution of electric field in the longitudinal direction can be reduced by introducing tuner plates between the stems to reduce the non-uniformity to an acceptable limit of ±3%.

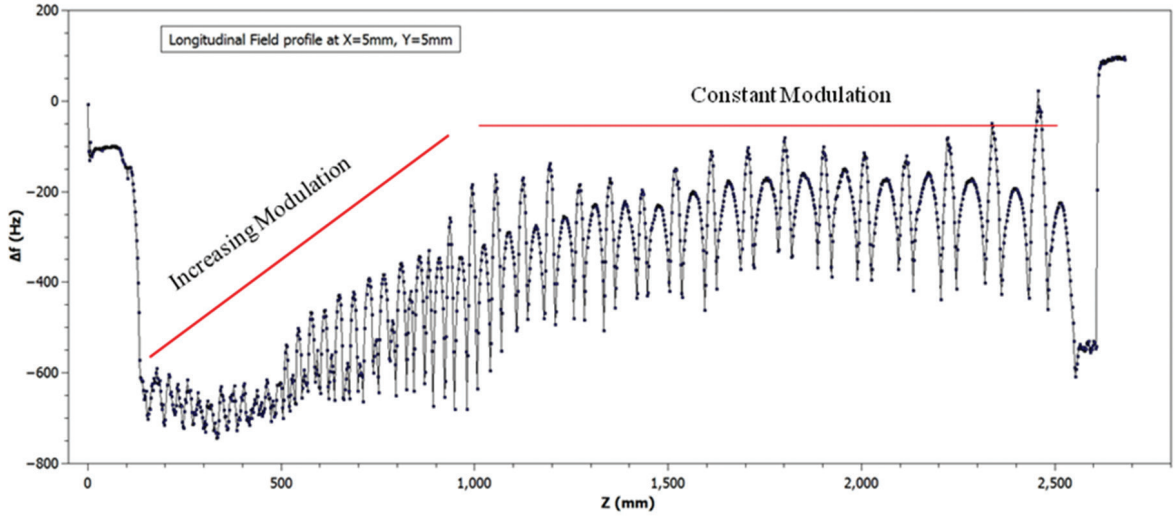

Fig 2.1.7 Longitudinal electric field profile obtained by placing dielectric bead inside the bore of electrodes and moving it along the beam axis in extremely small steps.

The modulated RFQ provides a bench to perform high power tests. Bead pull measurement has provided useful results. Quality factor Q and resonant frequency have been measured to be 5524 and 44.12 MHz respectively. The shunt impedance R derived from R/Q measurement using capacity variation method is found to be 87 k-ohm. The asymmetry in the electric field distribution in the four gaps was also measured. Distribution of the electric field was found to be symmetrical within the beam radius and tends to be asymmetrical in outer region.

2.1.3 Drift Tube LINAC Resonator

Ajith Kumar B P, J. Sacharias, R Mehta, V VVSatyanarayana, R V Hariwal, S Kedia, Rajesh Kumar, S. Venkataramanan, B K Sahu and P Barua

After the successful completion and design validation of the first DTL cavity the fabrication of the remaining five cavities started. The second tank has been fabricated and its assembly is over. Presently low level RF tests and bead pull test are underway. The second cavity consists of bunching section and accelerating section. The accelerating sections in the IH tanks are designed for 0° synchronous phase. The beam is injected into the accelerating sections with a reduced phase spread and velocity higher than the design velocity so that the bunch drifts to more negative phases during acceleration and emerges with a reduced energy spread. Short -60° sections at the entrance of the accelerating tank provide longitudinal focusing to allow matching to the next accelerating section. Figure 2.1.8 shows the second cavity.

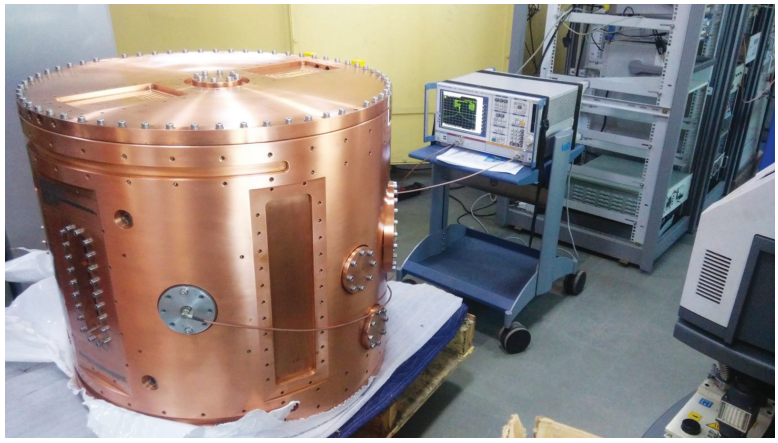

Fig. 2.1.8: Second DTL Cavity

2.1.4 Travelling wave chopper

S Kedia, Rajesh Kumar and R Mehta

The planned Travelling Wave Chopper (TWC) for the High Current Injector (HCI) has four pairs of deflecting plates (Figure 2.1.9) to produce desired chopped beam. The TWC will have variable frequency operations (@ 4 MHz, 2 MHz, 1 MHz, 500 kHz, 250 kHz and 125 kHz) to meet the pulse characteristics as required by the experimentalist. The pulse width is governed by the MHB parameters. The square pulse was chosen instead of square wave type pulse to maximize the efficiency and minimize the dark current/tailing effect. The successive plates of TWC are separated by 15 mm hence the chopping field must be synchronous with deflecting plate intervals. The electric field across each plate required to produce the desired deflection necessitates the use of four rectangular pulse pulsars working simultaneously and synchronously.

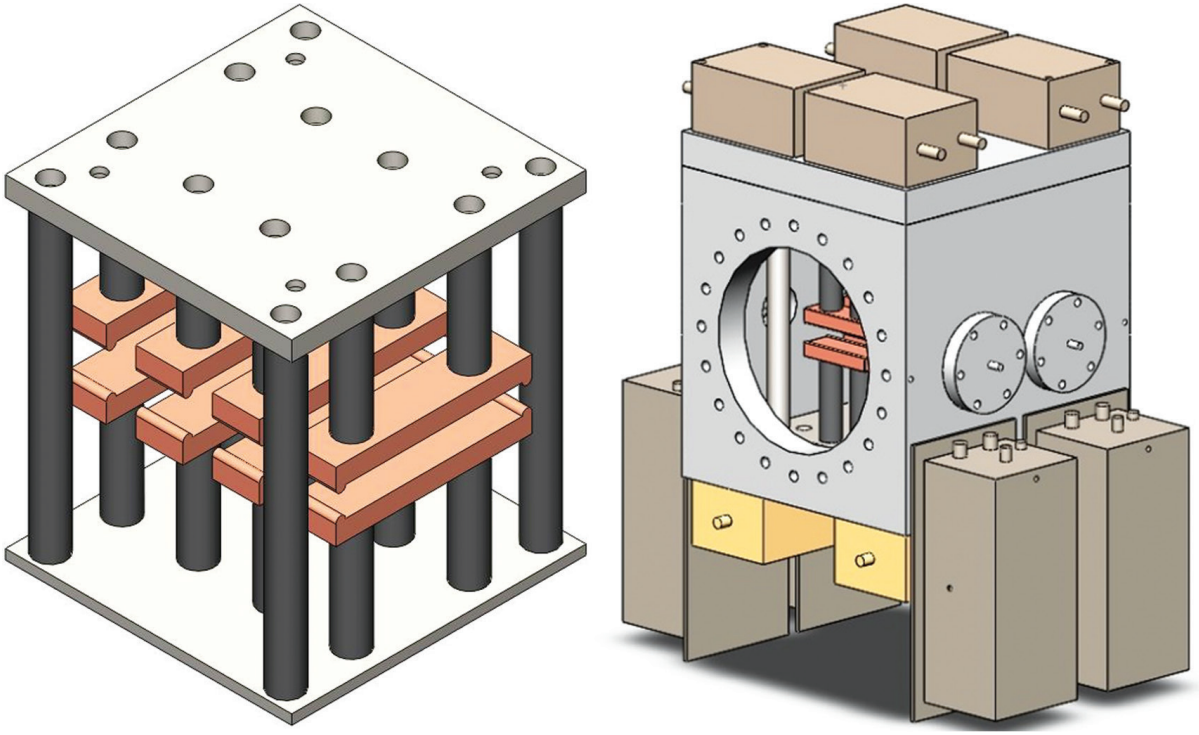

Fig. 2.1.9 The Travelling wave Chopper (right) the inner assembly and (left) the outer chamber with pulsers and power supplies

The possibilities of Chopper and TWD have been studied in various energy sections (LEBT, MEBT, HEBT). The LEBT was found to be most appropriate section for the Chopper and TWD, since it needs lower voltage to deflect the undesired particles. The existing LEBT section was modified accordingly (Figure 2.1.10).

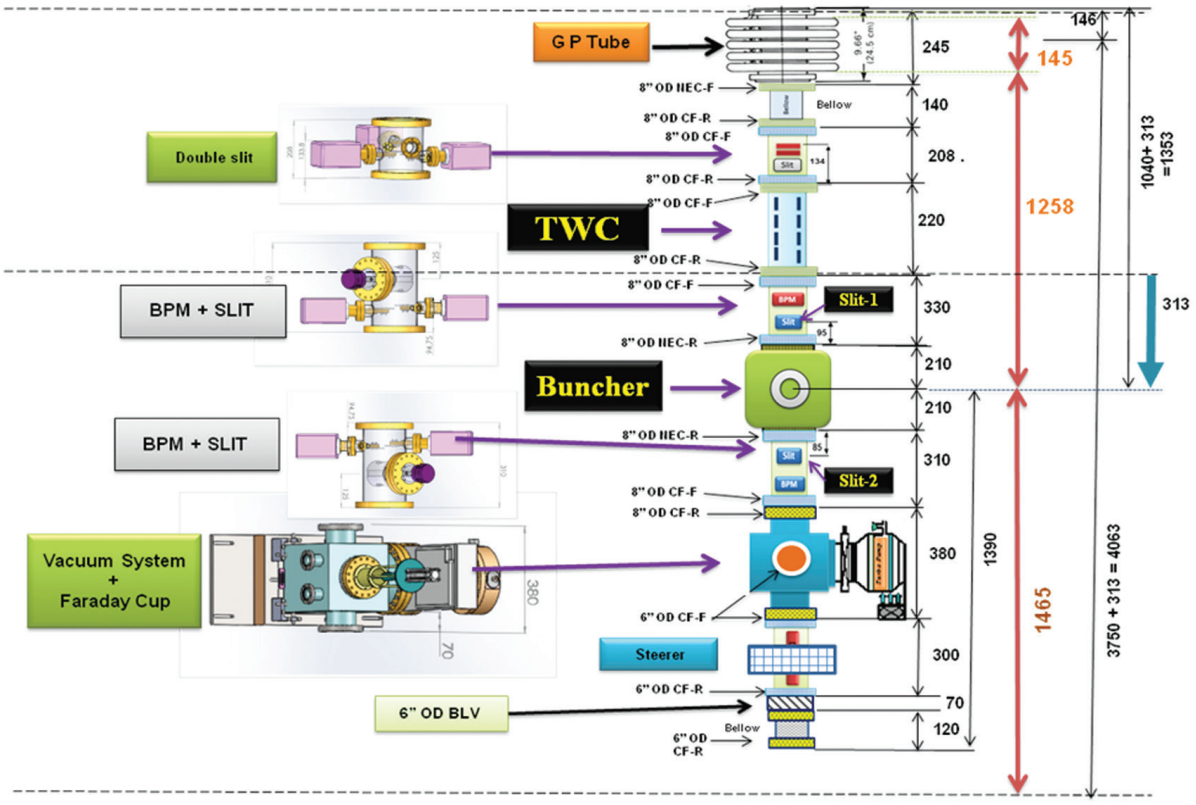

Fig. 2.1.10 The Modified Low Energy Beam Transport (LEBT) Section

Due to space constraint in the LEBT section, TWC has been designed within 220 mm space length along the beam line. The most outstanding feature of the design is multi-plate structure with increasing gap between the plates. The physical design of the TWC was carried out, which includes the four pairs of plates, length of plate, gap between the plates and slit to cut the undesired particles. To maximize the effective field, the gap between the plates was varied from 15 mm to 24 mm. The length of plate has been chosen in such a way that the current is maximized. The loaded capacitance of the structure was brought down to ~10 pF to achieve fast rise/fall time. The delay between set of plates has been kept constant.

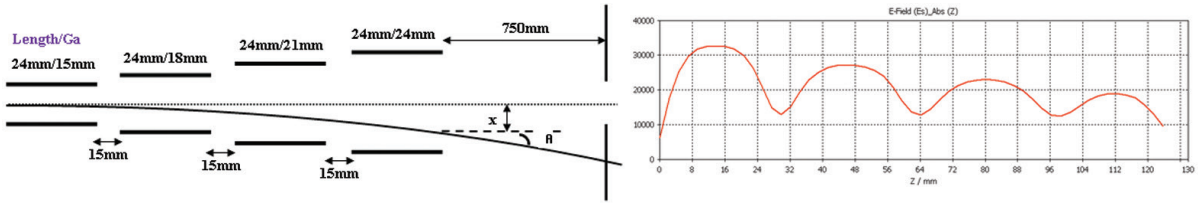

Fig. 2.1.11 Deflecting Plates and CST output of Electric Field

For the simplicity of calculations, the deflection and deflecting angle of beam due to deflector was calculated by the following equations, derived for parallel plate [1]

$$\theta \approx \frac{q\Delta VL}{Ag\beta^2 E_{0p}} ; x \approx (\frac{L}{2} + L_{drift})\theta \quad (1)$$

where θ is the deflecting angle at the exit of the deflector, x is the displacement at the exit of the deflector, ΔV is the deflecting voltage, g is the gap between the plates in mm, L is the length of plate in mm, E_{op} is the rest mass energy of proton, A is the mass in amu, β is the normalized velocity (v/c) and L_{drift} is the drift length after the deflector in mm.

Simulation Results

To validate the physical design of TWC various codes were used. The effective electric field was calculated using CST MWS. Two possibilities of slit locations have been explored after the TWC to cut the undesired particle. First one before MHB at 330mm away from the TWC and second one after MHB at 750 mm away from the TWC. A program has been developed in Python to verify the design. A simulation was carried out to check the feasibility of both locations. The TRACE 3D also validates the phase space ellipse obtained by Python codes (Figure 2.1.12a). The voltage required to deflect the undesired particles is 700V and 500V at slit location-1 and slit location-2 respectively. The phase space ellipse at slit location-2 seems to be better option as it provides better transmission and no tailing effect (Fig. 2.1.12b). The comparison between theoretical value, Python code and CST MWS were carried out. The amount of deflection at the both slit location has been tabulated (Table-2).

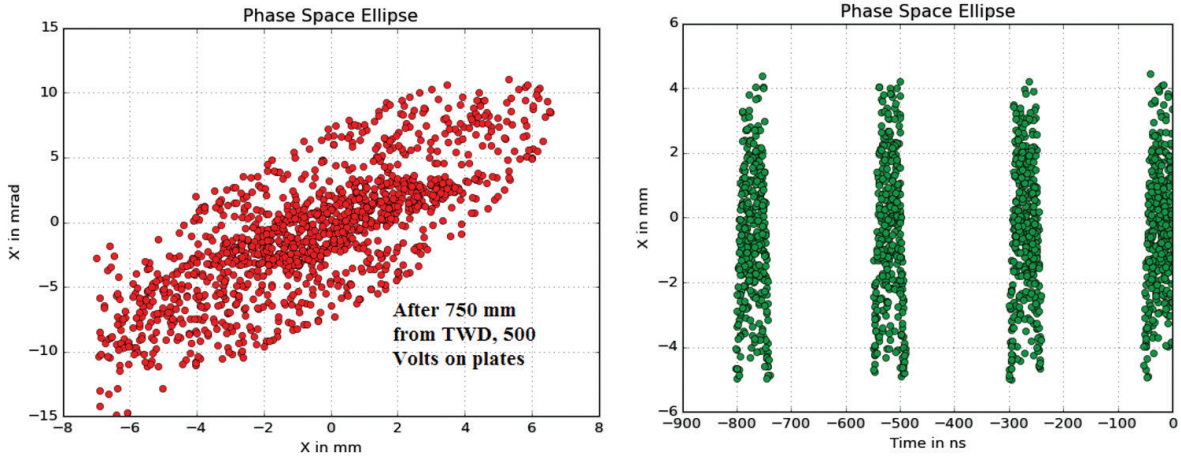

Fig. 2.1.12 Results obtained from python codes: (a) phase space ellipse at slit location-2, (b) pulsed beam at slit location-2.

Table 2: Amount of deflection at both slit locations:

	Theoretical Calculation	Pythons Codes	CST MWS
Slit Locatio-1	15	15.5	14.6
Slit Locatio-2	22	21.5	20.8

2.1.5 48.5 MHz Spiral Buncher for MEBT Section of HCI

R Mehta and R Ahuja

In order to match the longitudinal beam characteristics between the RFQ and the DTL, a buncher cavity is required. As the velocity is low, it was decided to go with a two-gap spiral buncher operating at 48.5 MHz, though its physical dimensions are comparatively large than at 97 MHz. The spiral is shorted to the tank at the root and the drift tube is mounted on the other end at the center of the spiral.

The buncher has been fabricated and resonance frequency was measured as 48.30 MHz under atmospheric pressure conditions, which matches very well with the designed frequency. The chamber was successfully copper plated at CSIR-Central Electro Chemical Research Institute (CSIR-CECRI), Karikudi, TN.

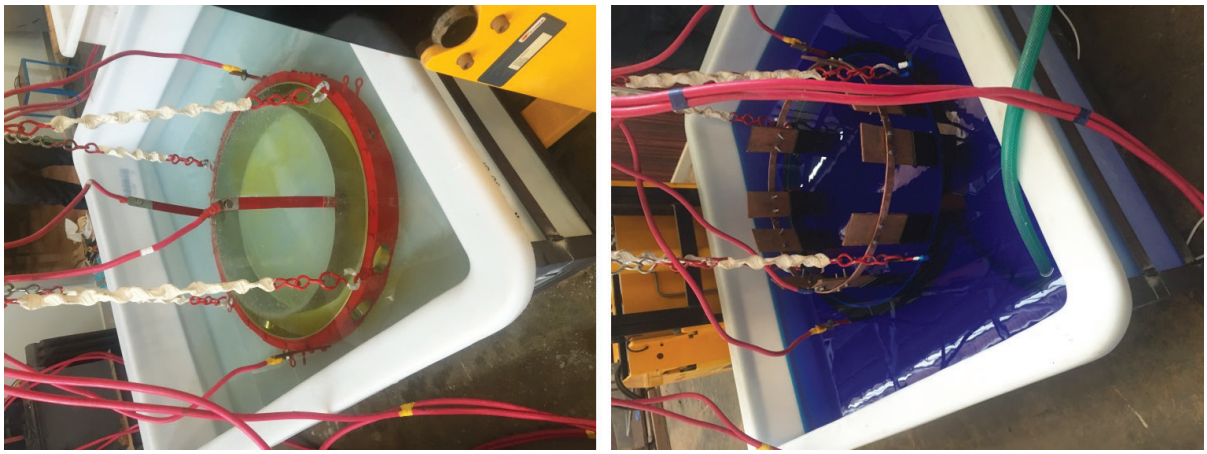

Fig. 2.1.13 Various stages of copper plating at CSIR-CECRI

Fig. 2.1.14 Copper Plated Surfaces

2.1.6 Beam Transport system for HCI

Sarvesh Kumar and A Mandal

This year a major thrust has been given for the finalization of the Low Energy Beam Transport (LEBT) Section of HCI in terms of beam optics layout and final installation of the components. The beam optics of LEBT is modified to incorporate a travelling wave chopper (TWC) before multi harmonic buncher (MHB). The main purpose of chopper is to change the repetition rate of ion beam. The magnetic quadrupoles before RFQ are tested with new XYZ scanner setup for field mapping. The beam optics is modified for magnetic quadrupoles as point to parallel to point configuration. This gives extra space to put a magnetic steerer in between the quadrupoles for steering of beam inside RFQ. All the magnets of high energy beam transport (HEBT) section have arrived to IUAC after testing at Danfysik, DENMARK.

2.1.6.1 Modified Beam Optics of LEBT section of HCI

The beam is extracted using an Einzel lens (EL) and a magnetic quadrupole singlet (MQS) and is analyzed using a large acceptance analyzing magnet (AM). To meet the demand from nuclear physics community for providing

pulsed beams at repetition rates of 250 ns to 8 µs, a TWC is being planned before MHB. To accommodate the TWC, one accelerating tube (AT) will be removed and the TWC will be placed before MHB. It has increased the distance between the analyzing magnet exit to MHB entrance by 303 mm from the original configuration. Accordingly, it is necessary to redo the ion-optics calculations. In the modified version of the beam optics design, the combined focusing action of the electrostatic quadrupole triplet (EQT) and one accelerating tube results in the magnification of beam size more than unity and thus the twiss parameters at the LEBT output are difficult to match exactly those of RFQ at its entrance using the original configuration of magnetic quadrupoles. The configuration of four quadrupoles has been changed to point-parallel-point configuration to match beam parameters of RFQ exactly. This gives enough space to incorporate a magnetic steerer between the magnetic quadrupoles which will help to steer the beam back to the central trajectory if needed inside RFQ. The beam optics for LEBT section along with RFQ is shown in Figure 2.1.15

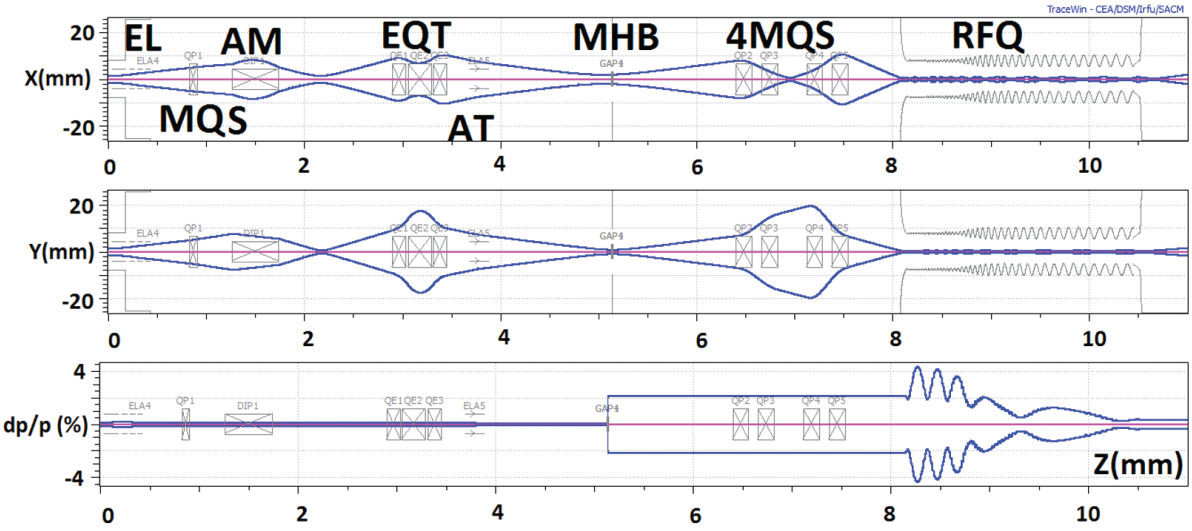

Fig. 2.1.15 Beam dynamics simulations of LEBT using TRACEWIN code

2.1.6.2 Commissioning of XYZ scanner and preliminary field mapping results

The XYZ scanner has been assembled, installed and is tested for field mapping of accelerator magnets. The air cooled magnetic quadrupoles and magnetic steerers of LEBT section have been tested. The field is mapped with in pole gap over the entire lenegth of the magnets. The effective lengths are calculated and found to be within ± 1mm of the deisgn value. Test results are shown in Fig. 2.1.16a and 2.1.16b for quadrupole and steerer magnets.

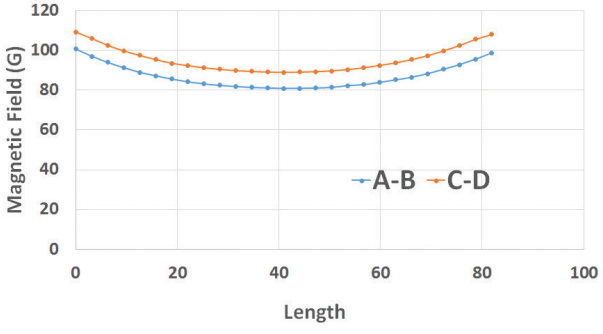

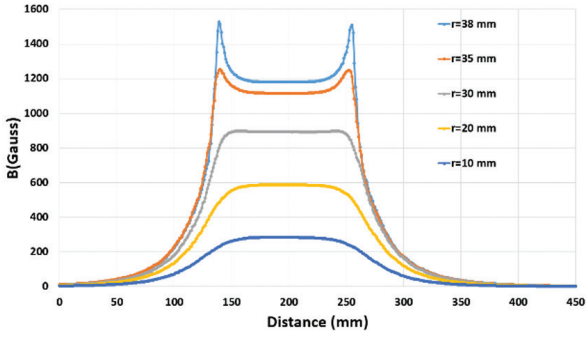

Fig. 2.1.16a Field mapping of SM for different planes Fig. 2.1.16b Field Mapping of MQ at diff. radius

2.1.6.3 Test results of magnets of HEBT section of HCI

All the dipole and quadrupole magnets for HEBT section of HCI have been tested at factory to get the design parameters. The test results agree well with the design values. All the quadrupole and dipole magnets are ready for final installation. The field homogeneity in the middle of the magnet is evaluated at maximum current as well as at 20% current, and is found to be 0.0004, for x<30 mm, at these currents. The dipole magnets (DM) are tested to determine effective field boundary (EFB), field homogeneity as shown in Figure 2.1.17a and 2.1.17b. The edge angles are with in ±1° of specified values and field homogeneity is of the order of 10^{-3}.

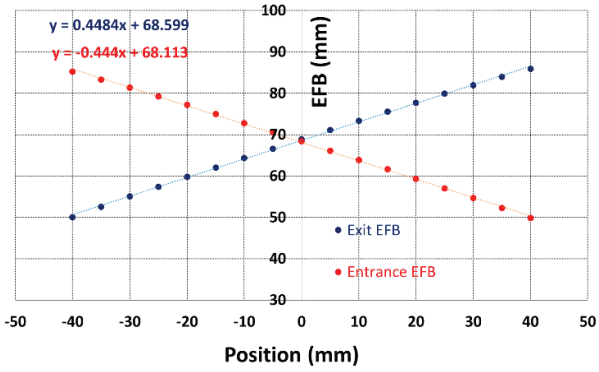

Fig. 2.1.17a: EFB on entrance and exit side of the DM

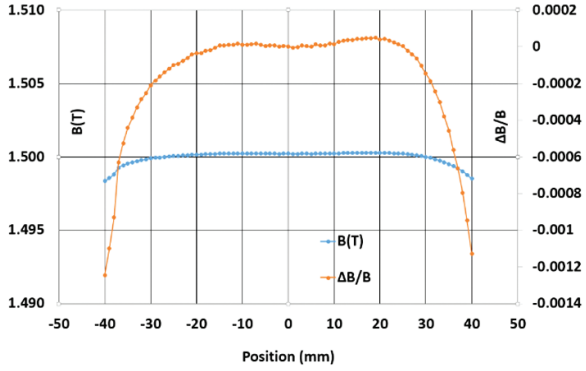

Fig. 2.1.17 b: Field homogeneity inside DM

There are basically four types of quadrupole magnets in HEBT namely, Q106, Q159, Q212, Q318 designated with their effective lengths in mm. The quadrupoles are tested for their magnetic center offset from the geometrical centre and the offset is found to be within ±0.1 mm in both X and Y directions. The test results are summarized in Table 1. For Q159, the field mapping is shown in Figure 2.1.17c. Harmonics measurements are being performed with respect to quadrupole component using rotating coil method. The total harmonic content is found to be ≤ 1% for all the quadrupole magnets. The measured higher order multipole contents are shown in Figure 2.1.17d with simulation results from OPERA 3D code.

Table 1. Test results of MQ in HEBT section

Magnet Type	Q106	Q159	Q212	Q318
Harmonic Content (%)	1.00	0.63	0.67	0.39
Offset (mm) (ΔX, ΔY)	0.04, -0.03	0.07, -0.05	0.06, 0.02	0.03, -0.01
Power (kW)	12.2	14.0	16.7	22.4
Leff.(mm)	106.4	159.9	212.9	318.7

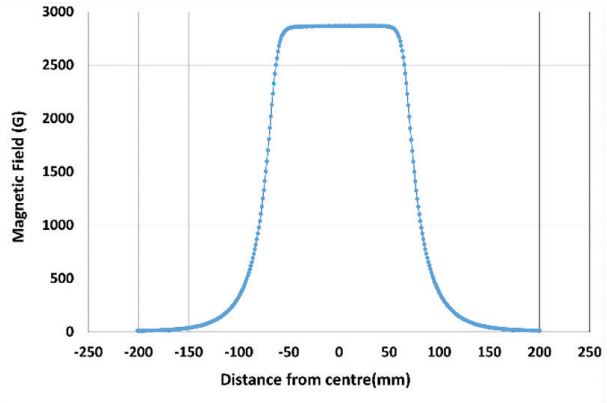

Fig. 2.1.17c: Longitudinal field mapping for Q159 magnet

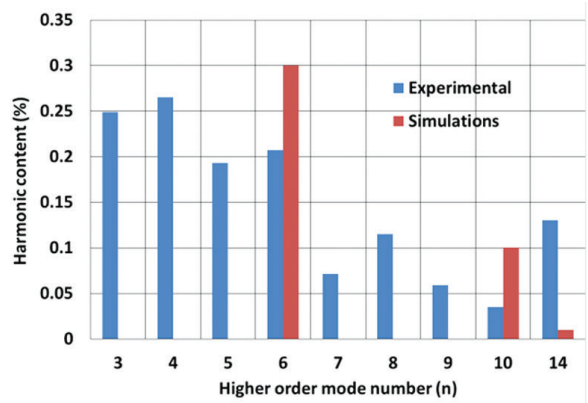

Fig. 2.1.17d: Harmonic contents for Q159 magnet

2.1.7 Instrumentation development

2.1.7.1 Development of Low Level RF (LLRF) Control System for DTL and RFQ

S. K. Suman V. V. V. Satyanarayana, Rajesh Kumar, R Mehta and BP Ajith Kumar

The development of LLRF control system for DTL and RFQ cavities has been started in-house. The architecture of the control system will be identical for all the six DTL cavities operating at 97 MHz, RFQ operating at 48.5 MHz & spiral buncher operating at 48.5 MHz frequency. The LLRF control requirements have been grouped into four units namely, Amplitude and Phase Control Loop (APCL), Frequency Tuner Control (FTC), Cavity Temperature Control (CTC) and RF Measurement and Diagnostic (RFMD). The RF signal processing is done using analog RF devices from "Mini Circuits", while the set points, read-backs, interlocking are done using digital circuits. The following units have been prototyped.

Amplitude and Phase Control Loop (APCL)

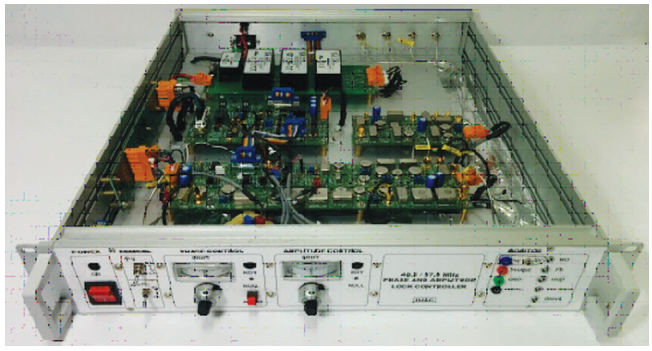

The designed controller is a Generator Driven fully analog control, based on Amplitude and Phase (A&P) control scheme. PI type analog feedback control loops are used to control the amplitude and phase of the cavity field. The amplitude control range 0-100% is from -30 dBm to 0 dBm, amplitude drift correction range is measured within ± 3 dBm and the phase drift correction range is ± 135°. The amplitude and phase control unit was tested with the DTL cavity up to 2kW RF power and amplitude and phase of the DTL cavity was controlled within 0.07%. It could not be tested at higher powers due to the temperature related frequency jitters. Mechanical frequency tuner and the temperature control were not available during this test.

Frequency Tuner Control (FTC)

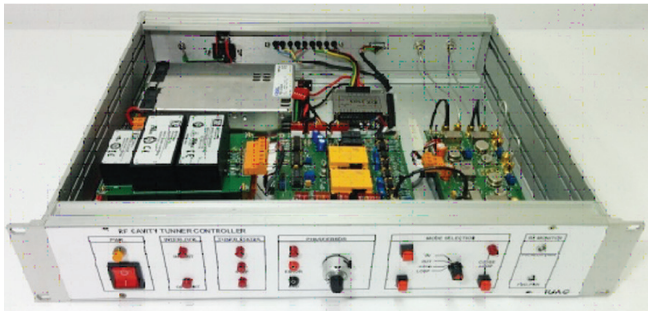

A closed loop controller to operate the mechanical tuner of the cavity has been designed and assembled. The controller has been tested on bench and is ready to be used with the cavity. The phase difference between the forward power and the pickup signal from the cavity is taken as an indicator of the cavity frequency detuning. It is an on/off type control based on bipolar window comparator to keep the phase error within acceptable limits. These limits are adjustable according to the need for sensitivity and stability. The controller has been provided with close and open loop operation and can drive both stepper as well as servo motors. The tuner operation is inhibited if the cavity field is too small. Tuner movement reversal, enable / disable and extreme position limit switches are provided to make the tuner operation safe. The operation of the mechanical tuning loop is very much influenced by the temperature of the cavity.

Cavity Temperature Control (CTC)

The design of the cavity temperature control was taken up next. As the operation of the amplitude and phase control loop and of the frequency tuning loop is very much influenced by the temperature of the cavity, to utilize the full dynamic control rage of the amplitude, phase and frequency controllers, the temperature of the cavity needs to be regulated within 1°C. The temperature control will be achieved by controlling the flow of cooling water in close loop using an electronically controlled flow valve. A cavity zero field signal indicating a Rf power

loss will be used to stop or bypass the water supply to the cavity. This will prevent further cooling of the cavity during an RF trip, so that when RF power is restored little time is lost to get the required temperature to have the desired resonance frequency. The first prototype of the CTC is expected to be complete by August 2016. The near-term goal for the complete LLRF system is to design and assemble the first prototype of each unit to acquire useful operational and performance data to validate the design for final product implementation.

2.1.7.2 Multi-Harmonic Buncher (MHB) Controller

S. K. Suman, V. V. V. Satyanarayana and Rajesh Kumar

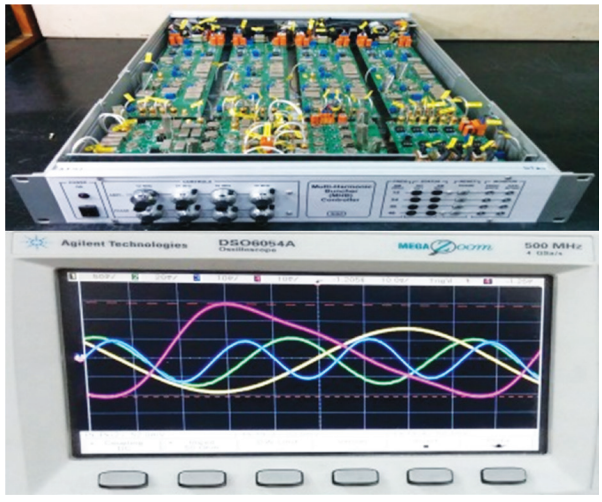

The controller generates 12 MHz saw-tooth of 70% linearity by combining 12MHz , 24MHz, 36MHz and 48MHz as per the expression V(t) = Vm (sin ωt - 0.40 sin 2ωt + 0.18 sin 3ωt - 0.06 sin 4ωt). The first prototype of the controller was successfully tested last year with the Pelletron-Linac MHB tank. During its first operational test, the controller was able to lock the phase, amplitude and shape of the MHB field. Test results obtained showed a very good stability and reliability as well as the provided controls proves to be enough to optimize the beam bunch width. Based on the data acquired during testing related to performance and functionality, the final product has been implemented with the required modifications. In the new design emphasis is placed on the hardware to suppress the EMI and ground loop problems, RF design rules are followed in the new PCB design. In addition to the local control a limited number of remote control operations are provided. The remote functions include master amplitude control, monitoring of amplitude and loop lock status of each harmonics. The expected completion date including preliminary testing in lab with dummy cavity is June 2016.

2.1.7.3 Pulsing Instrumentation for the TWC

Rajesh Kumar, S. K. Suman, V.V.V. Satyanarayana, R Joshi, S Kedia and R Mehta

The High Current Injector (HCI) utilizes a 4-plate Travelling Wave Chopper (TWC), required to produce precisely defined bunched beam. To select 60 ns beam bunch of 4 MHz repetition rate, every set of deflection plates will be driven independently by 4 MHz, 1 kV rectangular pulse of approximately 80% duty cycle (50ns low, 200ns high) having rise and fall time less than 10 ns. Since beam bunch delivery rates of 4 MHz down to 125 kHz are required, so only non-resonant type pulse generator will be used. Considering the trend in technology, use of MOSFET based push- pull configured pulse generator has been finalized.

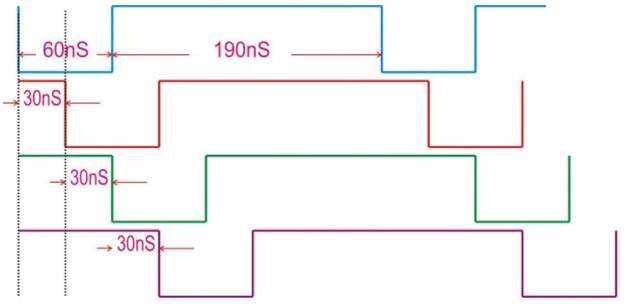

4MHz 1kV Synchronised Pulses across the four deflecting plates

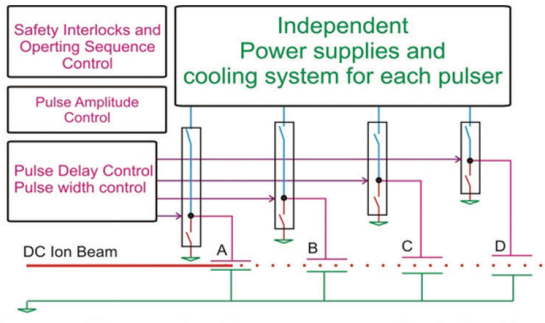

Layout of the required Instrumentation for the TWC

Efforts have been made to develop such pulsar in-house but without success, because of the cooling requirement which turns out to be unworkable with the available technique and within the required compact size. After meeting a dead-end in the in-house development possibilities, two companies: Ekspla and BEHLKE were contacted, which are supplying similar pulsars, but having no off-the-shelf products that were suitable for our application. These companies have been submitted with complete requirements in details and have been requested to give the best customized solutions for our application. BEHLKE has come up with better solution offering a single push-pull pulsar operating at 4 MHz, which is completely commensurate with our expectations: simple, reliable and more of a standard product. Initially instead of 4 pulsars only two pulsars will be bought to experiment the sensitivity problem between two adjacent pulsar channels. Further, the complete instrumentation for the TWC pulsing system will includes four main sections of instrumentation; the pulsars with required cooling system, required high voltage and low voltage bias power supplies, generation and synchronization of simultaneous pulses (Trigger unit) and the operation algorithm and safety control (control unit). Except the control unit, for rest of the units/ sections commercially available options will be used. The control unit will be developed in house as per the safety, operational and control requirements.

2.1.8 Compact Diagnostic Box

R. V. Hariwal, S Kedia and R. Mehta

The new design of the Compact Diagnostic Box (CDB) is circular in shape and it has two rectangular ports dedicated for Faraday cup and slit scanner respectively. A port for mounting the vacuum pump has also been provided. It has one 2.75" CFF port just opposite to the FC port for installing a capacitive pick-up to measure the bunch length of the ion beam at the entrance of the Drift Tube Linac (DTL) cavities. Two other 2.75" CFF ports shall be used for vacuum gauges and view port. This box can be mounted directly in front of the DTL resonator at the entrance without any external end flange which reduces the effective length of the CDB. The solid work drawings of CDB have been prepared for fabrication. The partial drawings and 3D model are shown in Fig 2.1.18.

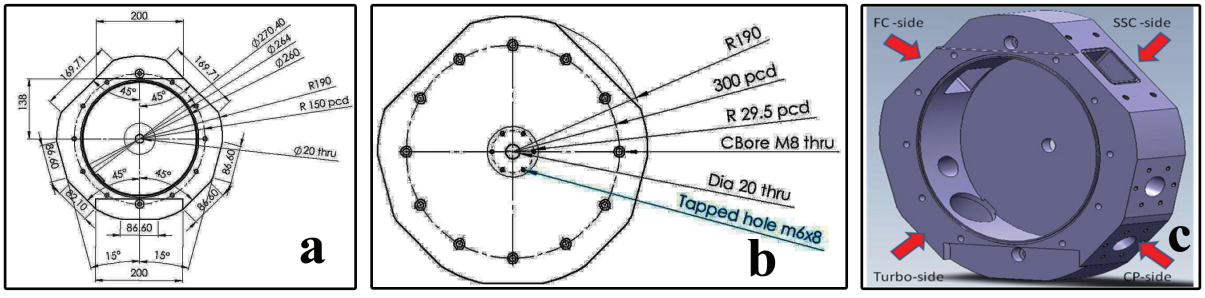

Fig. 2.1.18 (a) CDB front view (b) Back side view and (c) 3D model isometric view

Fabrication of the CDB is over. The turbo pump adapter is designed in such a way that it does not interfere with the DTL end flange. The CDB, along with its components, was mounted with the DTL resonator at the entrance flange and the respective PCD holes have been verified and matched. The CDB with FC, slit scanner, turbo pump adapter and DTL resonator, is shown in Figure 2.1.19.

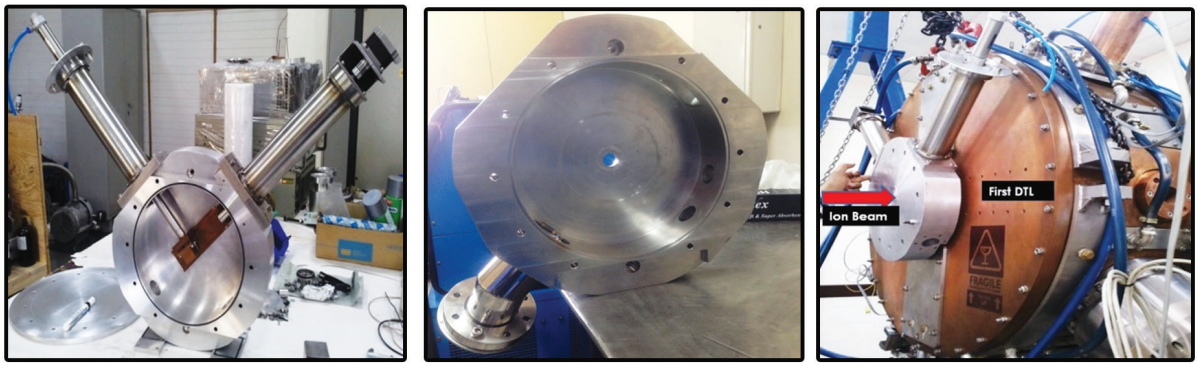

Fig. 2.1.19 (a) CDB with FC and slit scanner (b) turbo pump adopter (c) DTL resonator

The electronics design and control set-up to operate the motion of FC and slit scanner are under way. The FC is operated with the help of SMC air pneumatic cylinder CM2B25-60Z of 60 mm stroke length. The slit scanner linear motion is controlled by a stepper motor ARM69AC (oriental motor) of 2N-m torque. It travels approximately 70 mm in both directions. The slit scanner has two orthogonal slits of 300 micron width to measure the beam profiles with better resolution than previous one.

The capacitive pick-up is designed after the simulation of pick-up length for a given beam energy and its prototype is developed to fit within the compact diagnostic box. The pickup length and its aperture are optimized to 15 mm and 20 mm respectively. It was found from the simulation that the bunch length of the ion beam (β~0.05) is about 2 ns for the 15 mm pick-up length and 30 mm aperture configurations. The capacitive pick-up and bunch length measurement simulation are shown in Figure 2.1.20.

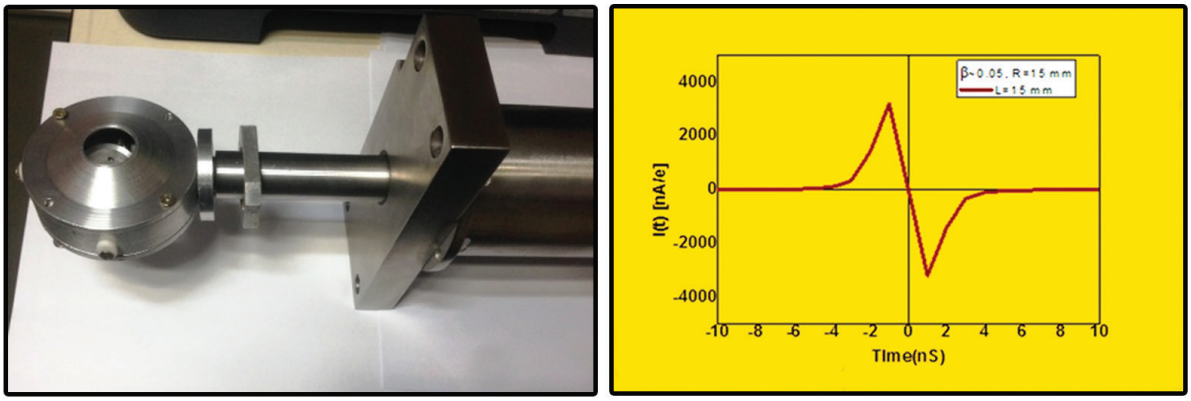

Fig. 2.1.20 (a) capacitive pick-up (b) Bunch length measurement

2.2 DEVELOPMENT OF AN ELECTRON ACCELERATOR

2.2.1 Delhi Light Source based on Free Electron Laser principle

S. Ghosh[1], J. Urakawa[2], N. Terunuma[2], S. Fukuda[2], M. Fukuda[2], A. Aryshev[2], B. K. Sahu[1], P. Patra[1], S. R. Abhilash[1], J. Karmakar[1], B. Karmakar[1], D. Kabiraj[1], N. Kumar[1], A. Sharma[1], V. Joshi[1], G. K. Chaudhari[1], A. Deshpande[3], T. Rao[5], V. Naik[4], A. Roy[4], R. K. Bhandari[1] and D. Kanjilal[1]

[1]Inter University Accelerator Centre (IUAC), Aruna Asaf Ali Marg, New Delhi, India
[2]High Energy Accelerator Research Organization, KEK, Tsukuba, Japan
[3]Society for Applied Microwave Electronics Engineering and Research, Mumbai, India
[4]Variable Energy Cyclotron Center, Kolkata, India
[5]Brookhaven National Laboratory, USA

2.2.1.1 Introduction

A project to build a compact Free Electron Laser (FEL) facility, named as Delhi Light Source (DLS), has been initiated at IUAC. In the first phase of the project, a high quality electron beam will be generated from a normal conducting (copper) photocathode electron gun which will be used to produce terahertz (THz) radiation by a compact undulator magnet. In the second phase, a superconducting electron gun will produce the electron beam for producing the THz radiation with higher average power. In the final stage of the project, the electron beam from the normal conducting or superconducting electron gun will be injected into the superconducting accelerating cavity to increase the beam energy from 8 MeV to 40 MeV which will be injected into long undulator magnets to produce Infrared radiation, and X-rays by inverse Compton scattering [1]. At present, the efforts are concentrated towards developing the first phase of DLS project.

The phase-I of the DLS project will be a pre-bunched FEL facility where the micro-bunch formation of the electrons will take place at the photocathode located inside the electron gun by striking with ultra-short laser pulses (time width of a few hundreds of femtoseconds). The laser pulse produced at a frequency of 5-50 Hz will

be split into many pulses (e.g. 2, 4, 8 or 16) and they will produce a 'comb beam' [2, 3] structure of electrons at the photocathode. There will be option to vary the separation of the laser pulses and thus the separation of the electron microbunches can be varied. The accelerating field in the electron gun copper cavity is expected to be ~ 120 MV/m which will accelerate the electron beam to an energy of ~ 8 MeV. The copper cavity will be followed by a normal conducting solenoid magnet to focus the beam at the center of a compact undulator magnet (length ≤ 1000 mm). The wavelength of the THz radiation produced from the electrons wiggling inside the undulator magnet will be equal to the separation of the electron bunches and this separation can be varied by changing the separation of the split laser pulses with the help of optical elements of the laser device. By adjusting the electron energy and the magnetic field of the undulator, the wavelength of the THz radiation can be varied in the range of ~ 0.15 to 2 THz.

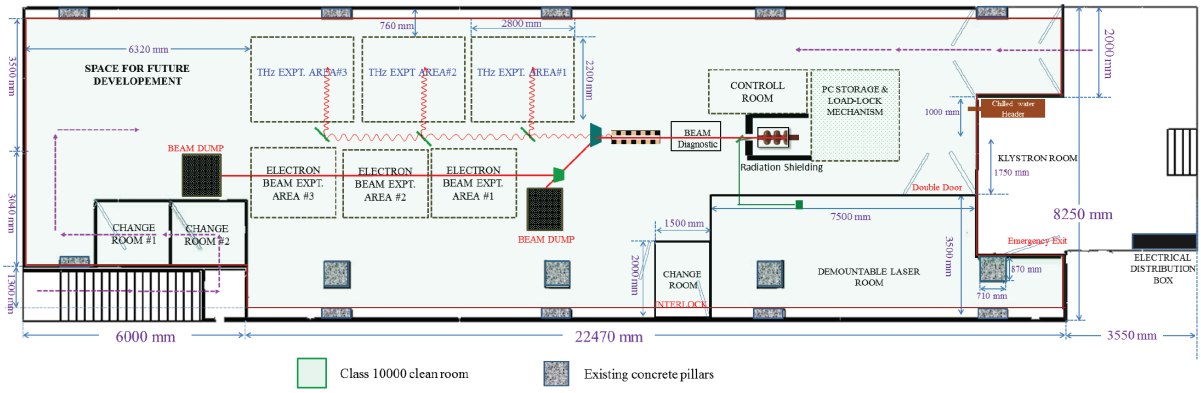

Fig. 2.2.1 Schematic layout of the first phase of DLS facility

2.2.1.2 Major components of the facility and their status:

The layout of the accelerator and experimental facility is shown in Figure 1. A class 10,000 clean room (28 m × 8 m) is being constructed to accommodate the entire accelerator and experimental facilities (Figure 2.2.1). Substantial progress has been made in many areas of Phase-I of DLS, as listed in the following:

RF electron gun

The resonance frequency of the RF gun was chosen to be 2860 MHz for a 2.6 cell copper cavity whose design is similar to those at BNL and KEK [4, 5]. The design and fabrication of the copper cavity (Figure 2) were done at KEK, Japan. Indian researchers from IUAC and SAMEER have participated in the activity. The results of the bead pull measurement data along with the electric field profile simulated from Superfish [6], is shown in fig. 2.2.2.

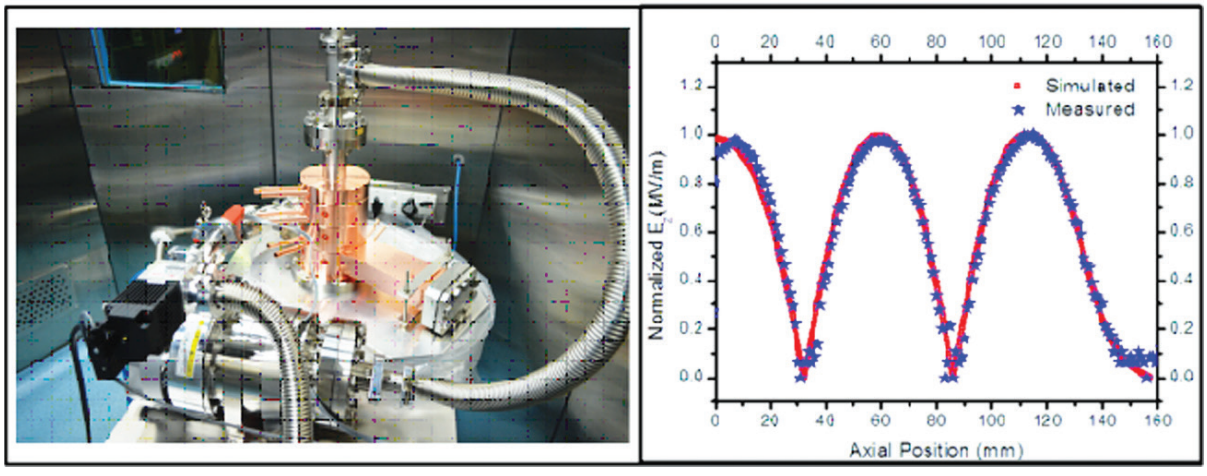

Fig. 2.2.2 2860 MHz copper cavity as RF gun and its electric field profile from Superfish and bead pull measurement

The RF system

The RF system for the Delhi Light Source consists of a high power klystron along with a suitable modulator and the low level RF system (LLRF). To meet the stringent beam requirement, the RF phase stability of 0.1 degree and amplitude stability better than 0.01% have been decided as the design goal of the LLRF system. The designed LLRF subsystem of the RF gun is composed of cavity controller with an amplitude loop and a phase loop operating in pulsed mode. A separate closed loop control to make the laser system synchronized with the cavity RF signal is also incorporated. The high power RF system consists of klystron tube, solid state modulator along with vacuum based wave guide components. The detailed specification of the high power RF system is given in Table-1.

Table 1 : Main parameters for klystron & modulator.

Parameter – RF system	Value
Peak Output power	≥ 25 MW
Average Output power	≥ 5 kW
Operating frequency	2860 MHz
Bandwidth (-1 dB)	± 1MHz
RF pulse duration	0.2 μs to 4 μs
Pulse repetition rate	1-50 Hz
Pulse top flatness	±0.3%
Rate of rise and fall of modulator output voltage	200-250 kV/μs
Long term stability	±0.05 %

Table 2. Proposed laser parameters

Laser System	**Energy/ Pulse at IR**	**Energy/ Pulse at UV**	**Pulse Width**
Fiber	> 200 μJ	> 20 μJ	300 fs
Fiber - assembled	> 250 μJ	> 25 μJ	< 200 fs
Hybrid	> 2 mJ	> 200 μJ	500 fs
Ti:Sa	> 10 mJ	> 1.5 mJ	100 fs

Table 3: Requirement of laser energy from Cu and Cs_2Te photocathode

Charge/ Pulse	**No. of microbunches produced**	**Laser Energy (UV) required at the PC**	
		Cu	Cs_2Te
6 pC	1	2.8 μJ	5.6 nJ
6 pC	2	6.3 μJ	12.6 nJ
6 pC	4	14.3 μJ	28.3 nJ
6 pC	8	32.0 μJ	64.0 nJ
6 pC	16	74.6 μJ	149.3 nJ

Proposed laser system for the photocathode

There will be a provision in the laser system to split each laser pulses into 2, 4, 8, 16 micro-pulses to generate a 'comb beam' structure of electron with the separation of a few hundreds of femtosecond (~ 2 × FWHM). In addition, the separation between successive micro-pulses is to be varied so that the THz radiation produced by the electron from the undulator magnet can be tuned. A few commercial laser systems, e.g. fiber, hybrid and solid state devices are currently being examined and the most appropriate one will be chosen shortly. The possibility to assemble a fiber laser device in-house is also being explored. Table-2 shows the output from four high power laser systems. The tentative laser energy required to produce the 'comb electron beam' of a nominal charge of 6 pC per microbunch from Cu and Cs_2Te photocathodes, is shown in Table-3, here the numbers correspond to pulse splitting in UV.

Photocathode (PC) preparation system

During the initial stage of operation of DLS, it is planned to use copper photocathode to produce high quality ultra-short bunches of electron beam. To produce Cs_2Te and the other advanced photocathode material, the design and development of the deposition chamber along with the provision of laser cleaning of the photocathode, storage chamber and its insertion mechanism into the RF cavity are presently going on. The complete deposition and transfer mechanism of the photocathode is planned to be carried out at a vacuum level of $\sim 1\times10^{-11}$ mbar.

Beam optics design using ASTRA code

The beam transport simulation is done using ASTRA code [7]. A few results of 8 microbunches with charge of 6, 12 and 25 pC/microbunch produced at the photocathode and transported up to the undulator magnet, are shown in Table 4. The effect of space charge force is observed in the simulation calculation due to the small time width of the electron bunches (300 fs). So, when the charge per microbunch is increased, more temporal separation between the successive bunches is necessary to avoid overlapping of the electrons. In the simulation, the major parameters used are:

a. Accelerating field of the cavity is 120 MV/m to produce > 8 MeV of electron beam.

b. At photocathode, the FWHM of the beam is 300 fs and their subsequent separations are optimized for 6, 12 and 25 pC of charge/micro-pulse by ensuring that at least 60% of the electron beams are not overlapped among the neighbouring bunches (Table 4).

c. Optimized launching phase for all three charges are 35° and the emittances are within 0.4 to 0.6 π mm-mrad.

Table 4. A few optimized parameters from Astra

Charge/ micropulse (pC)	Separation between microbunches	Solenoid Field (T)	Freq. Produced
6	500 fs	0.264	2 THz
12	650 fs	0.269	1.5 THz
25	800 fs	0.273	1.25 THz

Table 5: The tentative parameters of the undulator

λ_R in mm	Freq. produced (THz)	Electron Energy (MeV)	λ_U in mm	K Value	B_u (T)	Required gap (mm)
2	0.15	6	40	3.575	0.96	12
0.1	2	8	40	0.475	0.13	36

Compact undulator magnet

The preliminary calculation related to undulator magnet has been started. A realistic design of the undulator magnet to generate the photon frequency between 0.15 to 2 THz has been initiated for its wavelength (λ_U) and no. of periods equal to 40 mm and 20 respectively with a gap varying between 12 to 36 mm (Table 5). More time and effort are necessary to finalize the design of the compact undulator magnet.

2.2.1.3 Conclusion

The design, development, procurement of different subsystems of the Delhi Light Source is presently going on. The normal conducting RF cavity to be used as electron gun is already fabricated and tested with low power RF. The beam optics calculation is completed and the results will be used for simulation calculation to optimize the gain of the electromagnetic radiation produced from DLS (phase-I). The procurement process of the high power RF system including Klystron and Modulator is in the final stage. The parameter of the laser devices will be finalized within a few months and then the purchase procedure will be started. The design of the photocathode deposition system is on the verge of completion and commercial suppliers are being contacted to receive their feedback for fabrication. The design and selection of the beam line and the beam diagnostic components are presently going on. The production of electron beam and THz radiation are expected to be demonstrated by 2017 and 2018 respectively.

REFERENCES:

[1] S. Ghosh et al., Proc. of FEL2014, Basel, Switzerland, p. 596.
[2] S. Liu and J. Urakawa, Proc. of Free Electron Laser 2011, Shanghai, China, page 92-95.
[3] M. Boscolo et al., NIM A 577 (2007), page 409-416.
[4] X. J. Wang et al., Nucl. Instrum. Meth. A356, 1995, p. 159.
[5] A. Deshpande et al., Phy. Rev. Special Topic Accel. Beams, 14, 2011, 063501.
[6] Los Alamos Accelerator Code Group, Reference Manual for the Poisson/Superfish Group of Codes (Los Alamos National Laboratory, LA-UR-87-126, 1987).
[7] K. Flöttmann, ASTRA, www.desy.de/~mpyflo.

2.3 ECR AND MICROWAVE ION SOURCE DEVELOPMENTS

G. Rodrigues, Y. Mathur, Narender Kumar, Kedar Mal, P. Kumar, R. Ahuja, U. K. Rao & D. Kanjilal

A. 2.45 GHz microwave ion source developments

(i) Testing the performance of commissioned 2.45 GHz Microwave ion source based high flux system

A view of the compact 2.45 GHz microwave ion based, high flux system is schematically shown in Figure 2.5.1. The performance of 2.45 GHz microwave ion source based, high intensity, ion beam facility which has been installed and commissioned, has been tested by carrying out beam current measurements and X-ray measurements. The beam current measurements had been carried out on the compact experimental ladder mounted in a compact experiment chamber. The design of the compact experimental chamber and experimental ladder is shown in Figure 2.3.2.

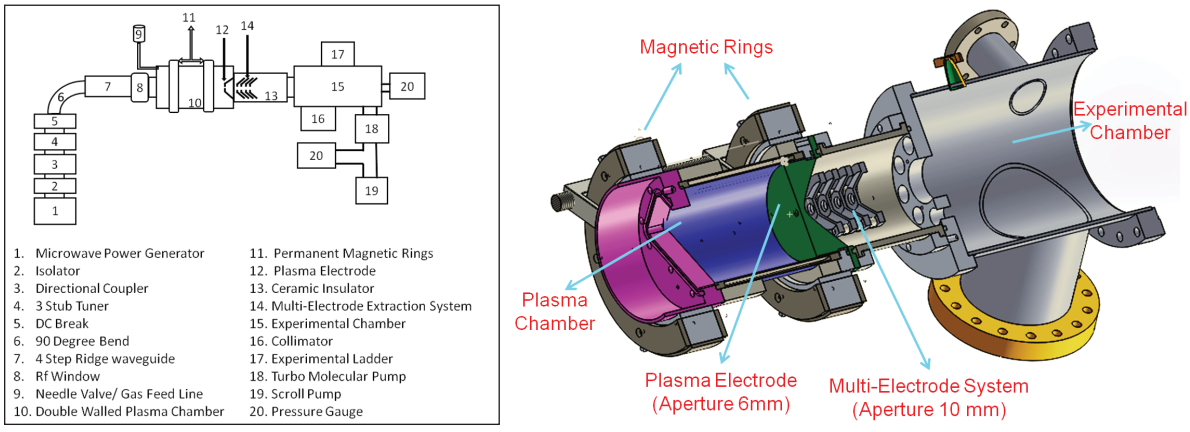

Fig. 2.3.1 (left) Schematic of the 2.45 GHz microwave ion source based, high intensity, ion beam facility ; (right) cross sectional view of the multielectode system coupled with plasma chamber

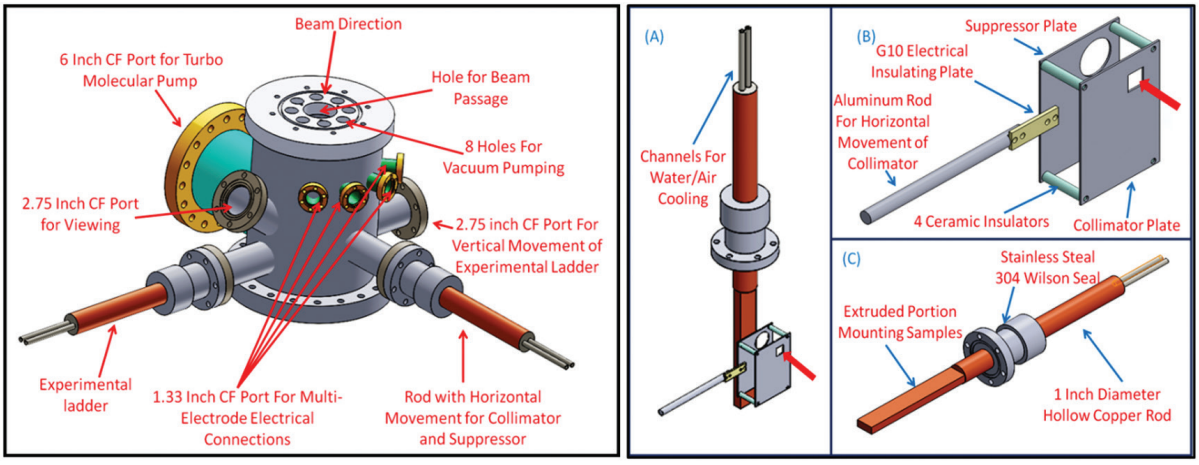

Fig. 2.3.1 (left) Schematic of the 2.45 GHz microwave ion source based, high intensity, ion beam facility ; (right) cross sectional view of the multielectode system coupled with plasma chamber

The ion beam intensity measurements were carried out by collimating the beam on the experimental ladder with the help of collimator plate (~typically beam area can be collimated from a few mm^2 to a few tens of mm^2). The highest intensity of the extracted hydrogen beam current for 10 kV extraction voltage was achieved around 210 $\mu A/cm^2$ for hydrogen gas pressure of 9.6×10^{-6} mbar. The total beam current per unit area measurements carried out for nitrogen gas for various microwave power levels and extraction voltages at gas pressure of 6.8×10^{-6} mbar is shown in Figure 2.3.3 [1]. This high flux system has been used for performing 10 keV nitrogen and oxygen ions implantation experiments on silicon for fluence variation from 5×10^{15} ions/cm^2 to 1×10^{18} ions/cm^2 [1]. The samples were characterized using Rutherford Backscattering spectrometry performed by 1MV Pelletron accelerator at IUAC.

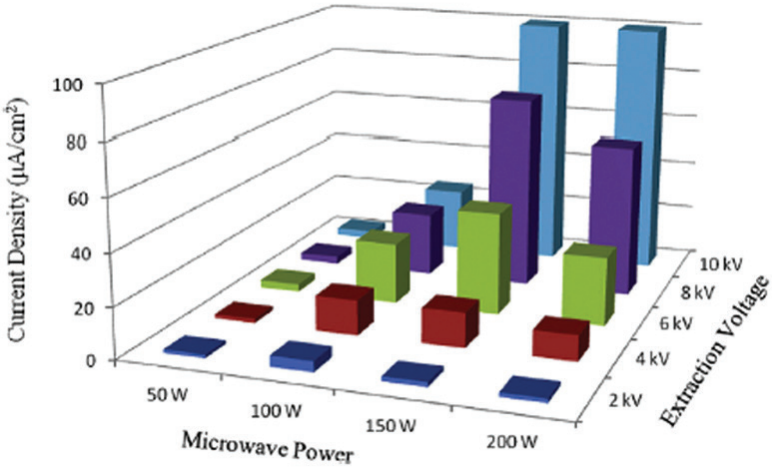

Fig. 2.3.3 Beam currents on experimental ladder for various microwave power levels and extraction voltages

(ii) X-ray measurements

In our earlier work, we have measured the X-rays as a function of the RF power, gas pressure and magnetic field and observed that high energy X-rays were evolved due to launching of the EM wave in the under-resonance region, which is not explainable by normal ECR heating.

Fig. 2.3.4 (left) shows the experimental set-up of the 2.45 GHz microwave ion source and position of the 3"x 3" NaI (Tl) detector to detect the X-rays in the radial direction. The view port through which X-rays were detected

was covered with a thin Mylar foil with a 5 mm diameter opening. The axial magnetic field is tunable by moving the permanent magnet rings to adjust the magnetic field (B_{inj}) at the location of the RF window. We assume that the wave is launched from the position of the RF window. The measurement of X-rays from the plasma has been undertaken by varying the magnetic field at the location of the RF window and studying the effect of the electromagnetic wave's launching position at a corresponding magnetic field on the electron energy distribution function of the plasma. The magnetic field at the RF launching position was varied by moving the injection ring only and keeping the extraction ring position fixed. The distance between the injection magnetic ring and the RF window was varied from 10.5 mm to 42.5 mm. Figure 2.3.4 (right) shows the variation in the total number X-ray counts of various energies measured using the NaI(Tl) detector with the variation of the magnetic field. Figure 2.3.5 shows the variation in the total number of counts per minute with the varying magnetic field at RF launching position.

It was observed that the mean electron energies were in the range of ~ 17 keV. The maximum X-ray counts were observed at $B_{inj}/B_{ECR} \sim 0.8$ and the X-ray intensities further diminished at higher values of B_{inj}/B_{ECR}. The conditions of $B < B_{ECR}$ and $n < n_{CUT\text{-}OFF}$ are favourable for X-B conversion and the absorption of the electron Bernstein wave at the first harmonic of ECR is possible. The conditions in the present measurement indicate that X-B conversion takes place during the launching of the RF wave in the under-resonance region and the resultant electron Bernstein waves are responsible for the relatively high electron energies observed. It should be mentioned that in earlier measurements, the beam intensity variation showed a similar trend with the X-ray measurements, indicating a plasma density enhancement. Langmuir probe measurements are required for measuring the plasma density to further confirm the enhancement of plasma densities.

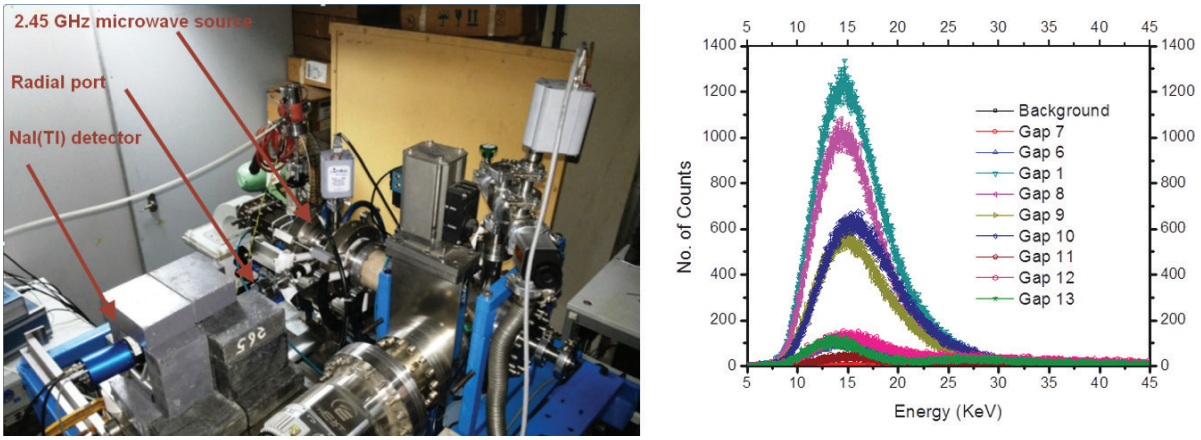

Fig. 2.3.4 (left) Experimental setup used for performing x-ray measurements and (right) plot showing variation in X-ray counts with variation of microwave power level (the X-ray counts are taken for 60 minutes in each case)

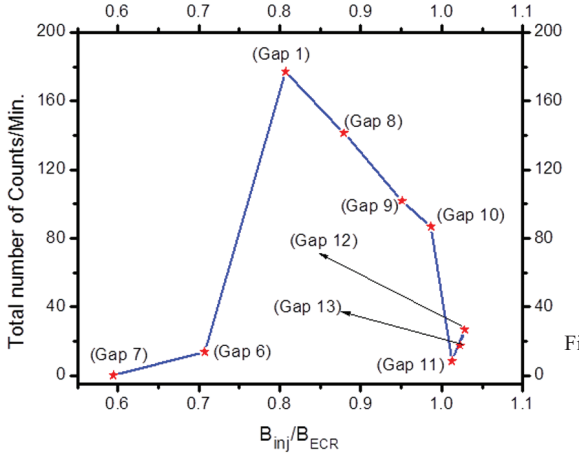

Fig 2.3.5 The variation in the total number of x-ray counts as a function of $B_{in}j/B_{ECR}$

B. Frequency tuning experiment using an aluminum bias tube in the 10 GHz NANOGAN ECR ion source

In previous measurements using a copper bias tube, we observed that the X-rays emitted towards the injection side were attenuated while traversing the copper bias tube (120 mm length). The statistics in the experimental data were quite poor to quantify the relationship between the observed X-ray counts and the beam intensities at various frequencies. To see the effect of frequency tuning on bremsstrahlung spectra with an aluminium bias tube (165 mm length), a new bias tube was fabricated and installed. The experimental measurements using frequency tuning effect was performed with argon beam, which is shown in Figure 2.3.6. The beam intensity, beam shape and bremsstrahlung spectra were measured as a function of frequency.

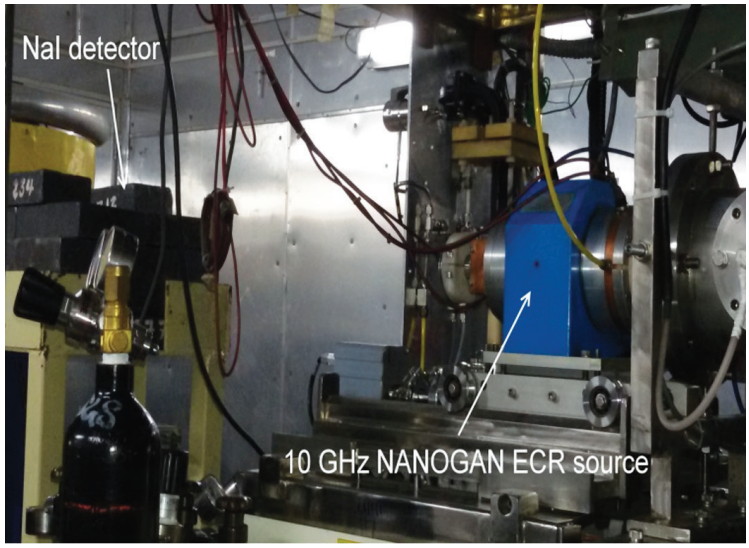

Fig. 2.3.6 View of the experimental set-up to detect X-rays at the injection side of 10 GHz NANOGAN ECR ion source as a function of frequency

(i) Beam intensity measurements and bremsstrahlung spectra

Frequency tuning has been carried out for mode optimization and various observed & calculated mode for argon plasma are shown in Figure 2.3.7. While tuning the frequency, the highest beam intensity of Ar^{9+} was observed at 8.56 GHz compared to other modes. Therefore, source was optimized for Ar^{9+} (~ 1.0 eμA) at 8.56 GHz and frequency was varied from 8.50 to 11.0 GHz (Fig. 2.3.8). The beam energy was 250 keV/q. The ion source parameters are given in the table 1.

Table 1. Source parameters at operating frequency of 8.56 GHz

Tuned frequency	8.56 GHz
Base vacuum (extraction side)	3.29 10^{-7} torr
RF power	38W, 4W, 20%, -1.97dB
DC bias voltage	-47 V, 0.060 emA
Extraction voltage	15 kV, 0.726 emA
Focus voltage	10.09 kV,0.0 emA
Platform voltage	235 kV, 0.43 emA
Main gas (Ar)	6.85 V
Support gas (-)	0.00 V
Injection vacuum (with plasma)	1.76 x 10^{-5} torr
Beamline vacuum	2.0 x 10^{-}8 torr
Total current (at first Faraday cup)	119 eμA
Source tuned for Ar^{9+}	1.10 eμA

Calculated modes from 8.50 to 11.0 GHz										
TE 115	TM 010	TM 011	TM 012	TE 116	TM 013	TM 014	TE 117	TM 015	TE 118	TM 016
8.621	8.826	8.891	9.082	9.324	9.393	9.811	10.091	10.323	10.910	10.917

Observed modes from 9.40 to 10.6 GHz for Argon Plasma (July 2013)											
9.60	9.67	9.72	9.81	9.95	10.00	10.13	10.23	10.30	10.39	10.42	10.53

Observed modes from 8.50 to 11.0 GHz for Argon Plasma (August 2015)												
8.53	8.56	8.78	8.86	9.08	9.21	9.25	9.34	9.38	9.56	9.62	9.69	9.74
9.78	9.83	9.92	10.02	10.10	10.22	10.42	10.55	10.60	10.71	10.81	10.85	10.89

Fig. 2.3.7 Calculated and observed modes from 8.5 to 11.0 GHz for argon plasma

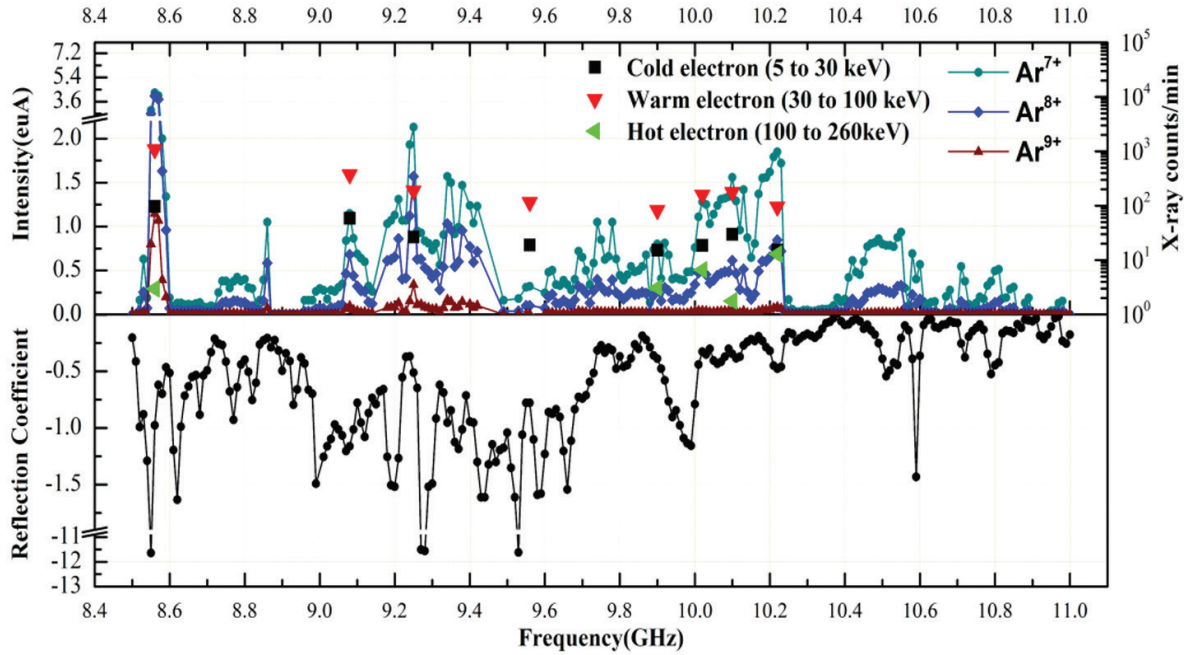

Fig. 2.3.8 Effect of frequency tuning on beam intensities of various charge states of argon and x-ray bremsstrahlung spectra

(ii) Beam shape measurements as a function of frequency

The beam shapes were digitized at selected frequencies when the intensities of argon beams were found high compared to the nearby frequencies. The digitized beam profiles at BPM -1 (before the analyzer magnet) are shown in Figure 2.3.9.

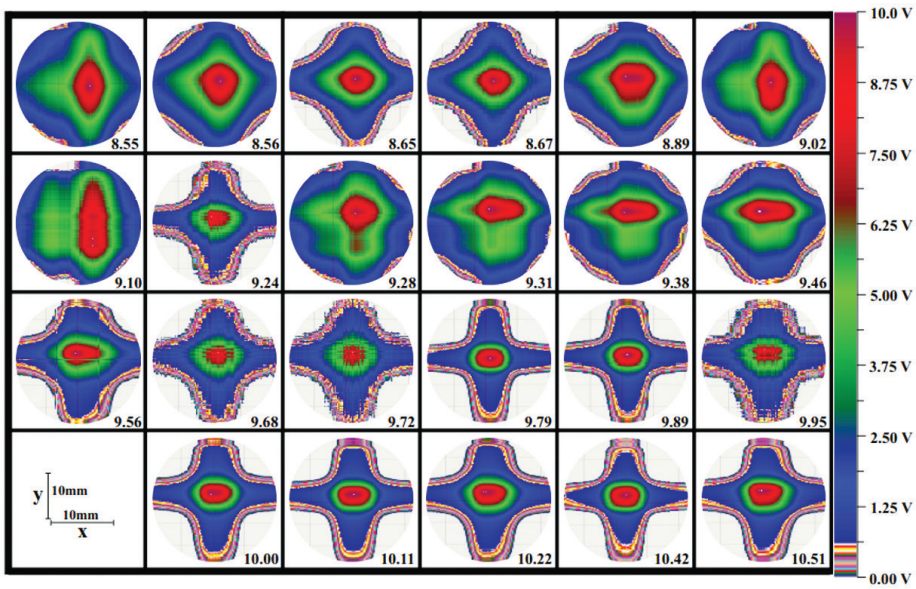

Fig. 2.3.9 Effect of the frequency on the beam shapes measured at BPM-1 (before analyzing magnet)

REFERENCES:

[1] Narender Kumar, G. Rodrigues, Y. Mathur, S. Ohja, R. Ahuja and D. Kanjilal, "Development and test of 2.45 GHz microwave ion source based intense ion beam experimental facility", Vacuum 124, 55-59 (2016).

[2] Narender Kumar, "High Flux 2.45 GHz microwave ion source", ID-386 (T-03), InPAC 2015, BARC, Mumbai.

[3] G. Rodrigues, N. Kumar, Y. Mathur, U. K. Rao and D. Kanjilal, "Alternative way of heating plasmas to increase the densities beyond their cut-off", ID-201, InPAC 2015, BARC, Mumbai.